

Hairline breakage detection in X-ray images using data fusion

C. Harriet Linda¹ · G. Wiselin Jiji²

Received: 7 March 2017 / Revised: 20 August 2017 / Accepted: 5 October 2017 /

Published online: 16 October 2017

© Springer Science+Business Media, LLC 2017

Abstract This paper deals with identification of hairline breakage in the X-Ray images. The crack in the X-Ray images can be missed due to absence of sharp edges and the intensity inhomogeneity. This work is carried out in two phases. In the first phase the preprocessing step is done using anisotropic diffusion filter and wavelet to preserve the edges and fine details. In the second phase Expectation Maximization (EM) algorithm is used for segmenting the image. The mask produced from the EM algorithm separates the bone region. The intensity variation calculation is performed over the selected region to detect the cracks. The performance of the proposed work is calculated using the parameters sensitivity and accuracy. This new approach is experimented with ten patient's data and validated by Radiologists. The performance of the proposed work is compared with recent works. This work greatly improves the accuracy of the segmentation on medical images and the overall accuracy is about 98%.

Keywords Anisotropic diffusion · Maximum likelihood estimation · Discrete wavelet transform · Expectation-maximization (EM) algorithm

1 Introduction

The X-Ray image is the most commonly used imaging modality for doctors to diagnose and treat bone diseases. The Fracture diagnosis, Evaluation of skeletal, Bone densitometry and Hip

✉ C. Harriet Linda
harriet_linda@yahoo.com

G. Wiselin Jiji
jijivevin@yahoo.co.in

¹ Department of Computer Science and Engineering, CSI Institute of Technology, Thovalai, Tamil Nadu 629 302, India

² Department of Computer Science and Engineering, Dr.Sivanthi Aditanar college of Engineering, Tiruchendur, Tamil Nadu, India

replacement are done based on the results of X-Ray images. The segmentation plays a vital role in computer-aided diagnosis, surgery and treatment.

The automatic detection of crack improves the timeliness and accuracy of diagnosis. The detection of cracks in x-ray images is a difficult and challenging. There are various methods [12] to detect fractures which leads to computer aided fracture detection. The crack detection in bone X-Ray images can be done by Fuzzy index measure [9]. The hairline mandibular fracture is detected using MRF-based approach [1]. The well displaced mandibular fractures are identified by Bayesian inference [6]. The hip fractures are clearly marked by the use of texture [17]. The femur bone fractures can be located using combined classifier approach [5], divide-conquer approach in SVM's kernel-space [10], neckshaft angle calculation [30] and combined detection methods [18]. The arm fractures are detected by the contour modeling coupled with shape constraints [13], the midshaft long bone fractures are clearly marked by the use of hough transform and gradient analysis [14], the bone fractures are detected by Artificial Neural Network Techniques [7] and fusion-based classification system [19] is used to detect the presence / absence of Tibia bone fracture(s) in medical images. The thresholding [27], edge-based [4, 29], region-based [8], graph-based [3] classification-based [31], and deformable model [22] are the most commonly used image segmentation techniques [24, 26] in different medical applications. Though there are lots of methods applied for detecting fractures on bone images, these are not sufficient to give accurate result. So it is necessary to introduce a new method to improve the accuracy to detect the fractures.

The proposed scheme is modeled as a two-step approach: preprocessing, hairline fracture identification using segmentation and intensity variation calculation. In the Preprocessing step, the 2D Anisotropic Diffusion filter [20, 23] along with Discrete Wavelet Transform [28] is used to remove the noises and to get the finite details. In the segmentation step the preprocessed image is segmented using Expectation Maximization algorithm [2, 16] to separate the bone region. Finally an intensity variation calculation technique is carried out to detect cracks. The performance is compared with some standard techniques such as “Automatic Crack Detection in Eggshell based on SUSAN Edge Detector Using Fuzzy Thresholding (FSUSAN)” [21] and “Crack detection in X-ray images using fuzzy index measure (FIM)” [9]. The experimental result shows that the proposed work identifies the crack well when compared to the standard techniques.

The remaining of this paper is organized as follows; Section 2 introduces the methodology involved in this paper. Section 3 describes the experiment results with analysis charts. A brief conclusion is given in Section 4.

2 Proposed method

The complete block diagram of the proposed method is shown in Fig. 1. After inputting an X-Ray image, we remove the noises and preserve the minute pixels using Anisotropic Diffusion filter and DWT. As a second step EM algorithm is used to separate the bone region and intensity variation calculation technique is used to detect the cracks. At section 2.1 we illustrate the preprocessing step involved to reduce noises and to preserve the minute details. After this step, section 2.2 describes the steps involved in Expectation Maximization algorithm. The section 2.3 describes how to separate the bone structure from the input image and section 2.4 describes the intensity variation calculation technique to detect the cracks.

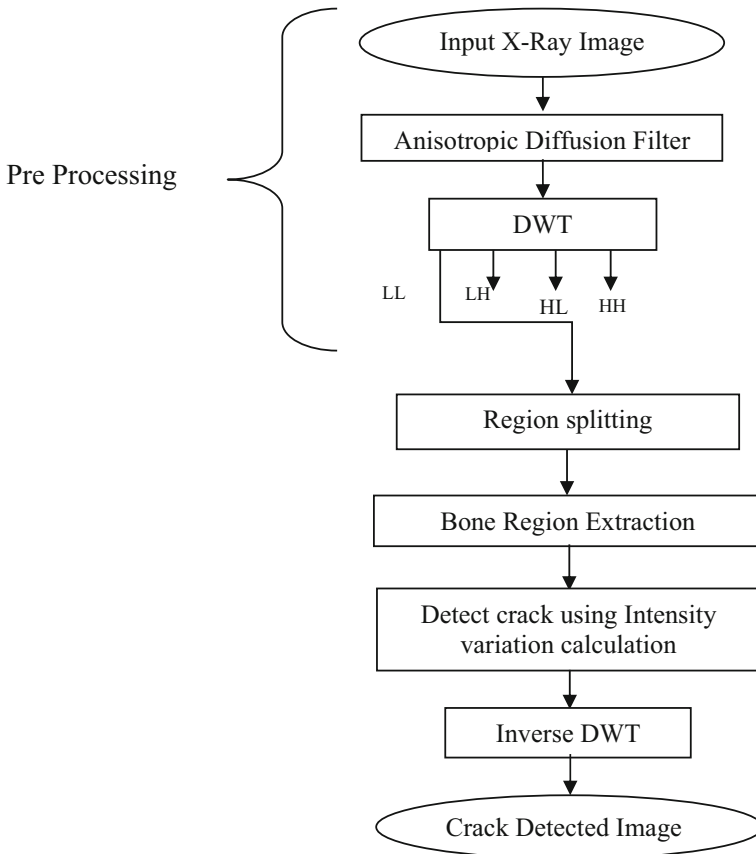


Fig. 1 Block diagram of the proposed work

2.1 Preprocessing

The preprocessing step is one of the essential steps in Medical images because noises are occurred in these images during acquisition. The denoising method is used in order to enhance the performance. In the proposed work, the 2D anisotropic Diffusion filter along with DWT is used for doing the preprocessing step. The detailed explanation of Anisotropic Filter is given in section 2.1.1. The section 2.1.2 tells the concept of wavelets. The main goal of this preprocessing step is to reduce noises, to enhance the edges and to retain the minute details.

2.1.1 Anisotropic diffusion

Any medical image is subjected to noises; these noises are removed by anisotropic diffusion filter. The purpose of the anisotropic diffusion filter is to improve the medical image quality by removing the noise and enhance the edges. Anisotropic Diffusion filter [20, 23] is able to retain the edges in the image by diminishing the noise in the non-homogenous region of image. Generally, the process can be represented in any dimension using the Eq. (1).

$$\frac{\partial}{\partial s} I(x, y, s) = \text{div}(f(x, y, s) \cdot \nabla I(x, y, s)) \tag{1}$$

where $I(x, y, s)$ denotes the image intensity, (x, y) be the spatial coordinate, s be the discrete implementation step and $f(x, y, s)$ denotes the diffusion function. Also ∇ is the gradient operator.

The diffusion function for the high contrast edges over low contrast one is expressed by the Eq. (2).

$$f(x, y, s) = e^{-\left[\frac{\nabla I}{E_{diff}}\right]^2} \tag{2}$$

where E_{diff} is the diffusion constant, which defines the value that triggers the smoothing process.

The diffusion function for wide regions over smaller ones is generally expressed as the Eq. (3).

$$f(x, y, s) = \frac{1}{1 + \left[\frac{\nabla I}{E_{diff}}\right]^2} \tag{3}$$

The 2D discrete information of anisotropic diffusion method forms the Eq. (4)

$$\frac{\partial}{\partial s} I(x, y, s) = \sum_{i=1}^8 D_i \tag{4}$$

where D_i represents the various eight neighborhood pixels, east, west, north, south, east-north, west-south, west-north and east-south. This D_i can be expressed in the form of the Eq. (5)

$$D_i = \begin{cases} \frac{k_i}{t_i} [p_i - I(x, y, s)] & \text{if } 1 \leq i \leq 4 \\ \frac{r_i}{(\Delta d)^2} [q_i - I(x, y, s)] & \text{otherwise} \end{cases} \tag{5}$$

where the values of k_i defines as

$$k_i = \begin{cases} g\left(x + \frac{\Delta x}{2}, y, s\right) & \text{if } i = 1 \\ g\left(x - \frac{\Delta x}{2}, y, s\right) & \text{if } i = 2 \\ g\left(x, y + \frac{\Delta y}{2}, s\right) & \text{if } i = 3 \\ g\left(x, y - \frac{\Delta y}{2}, s\right) & \text{otherwise} \end{cases} \quad 1 \leq i \leq 4$$

the values of t_i can be defined as

$$t_i = \begin{cases} (\Delta x)^2 & \text{if } i = 1, 2 \\ (\Delta y)^2 & \text{otherwise} \end{cases} \quad 1 \leq i \leq 4$$

the r_i values are calculated from the equation

$$r_i = \begin{cases} g\left(x + \frac{\Delta x}{2}, y + \frac{\Delta y}{2}, s\right) & \text{if } i = 5 \\ g\left(x - \frac{\Delta x}{2}, y - \frac{\Delta y}{2}, s\right) & \text{if } i = 6 \\ g\left(x + \frac{\Delta x}{2}, y - \frac{\Delta y}{2}, s\right) & \text{if } i = 7 \\ g\left(x - \frac{\Delta x}{2}, y + \frac{\Delta y}{2}, s\right) & \text{otherwise} \end{cases} \quad 5 \leq i \leq 8$$

the values for the p_i are defined as

$$p_i = \begin{cases} I(x + \Delta x, y, s) & \text{if } i = 1 \\ I(x - \Delta x, y, s) & \text{if } i = 2 \\ I(x, y + \Delta y, s) & \text{if } i = 3 \\ I(x, y - \Delta y, s) & \text{otherwise} \end{cases} \quad 1 \leq i \leq 4$$

and the q_i values defined as

$$q_i = \begin{cases} I(x + \Delta x, y + \Delta y, s) & \text{if } i = 5 \\ I(x - \Delta x, y - \Delta y, s) & \text{if } i = 6 \\ I(x + \Delta x, y - \Delta y, s) & \text{if } i = 7 \\ I(x - \Delta x, y + \Delta y, s) & \text{otherwise} \end{cases} \quad 5 \leq i \leq 8$$

Here, Δx , Δy and Δd are the relative distances, and these are considered as $\Delta x = 1$, $\Delta y = 1$ and $\Delta d = \sqrt{2}$.

The flow intensity contributed by its eight neighborhoods for each pixel in the image is given by the Eq. (6).

$$\frac{\partial}{\partial s} I(x, y, s + \Delta s) \approx I(x, y, s) + \Delta s \left[\sum_{i=1}^4 D_i + \frac{1}{2} \sum_{j=5}^8 D_j \right] \quad 0 < \Delta s < 1/7 \quad (6)$$

2.1.2 Wavelets

The wavelet transform [28] is significant to provide a solid description of images that are limited in spatial extent. It is very helpful in description of edge and line that are highly localized. In the DWT, the image is logically decomposed into different hierarchical sub-band system. The original image is decomposed into four sub-bands LL, LH, HL and HH. These four sub-bands are formed from the separate applications of vertical and horizontal filters. These four sub-bands are called finest scale wavelet coefficients. The LL sub-band produces the detailed image which has more minute details. Since the crack is a hairline breakage, the minute details are very important. So the LL sub-band is selected for further processing.

2.2 Region splitting

The x-ray image has background, skin and bone region, the region splitting plays a vital role to separate these regions for diagnosis. In the proposed work Expectation Maximization (EM) algorithm is used for segmentation. The EM algorithm [2, 16] is a procedure to calculate the maximum likelihood estimate by the iterative approach in the presence of hidden and missing

data. The Block diagram of the Expectation-Maximization Method is shown in Fig. 2. The EM algorithm consists of two major steps: an Expectation step (E-step), followed by a Maximization step (M-step). In the Expectation step, the missing data are estimated from the observed data and current estimate of the model parameters. In the Maximization step, the likelihood function is maximized under the assumption that the missing data are known. These E-step and M-step are iterated until convergence.

Consider the data set S of size n , $S = \{s_1, s_2, \dots, s_n\}$. The probability density function for the independent and identically distributed data vectors in $p(S|\alpha)$, and is defined by the Eq. (7).

$$p(S|\alpha) = \prod_{k=1}^n p(s_k|\alpha) \tag{7}$$

Where α be the set of parameters.

The Likelihood function with the parameter α and the data set S is $L(\alpha|S)$. The relationship between the probability density function $p(S|\alpha)$ and $L(\alpha|S)$ are expressed as the Eq. (8).

$$p(S|\alpha) = L(\alpha|S) \tag{8}$$

Our goal is to find the value of α that maximizes L . The maximum likelihood problem is defined as the Eq. (9).

$$\alpha^* = \operatorname{argmax}_{\alpha} L(\alpha|S) \tag{9}$$

Expectation step is necessary to find the expected value of the complete data log likelihood with respect to the unknown data T with the data set S and the present parameter estimates. This can be expressed by the Eq. (10).

$$Q(\alpha, \alpha^{k-1}) = E[\log p(S, T|\alpha) | S, \alpha^{k-1}] \tag{10}$$

where α be the new parameter and α^{k-1} be the present parameter estimates.

Maximization step is to maximize the expectation computed in the E-step by the Eq. (11).

$$\alpha^k = \operatorname{argmax}_{\alpha} Q(\alpha, \alpha^{k-1}) \tag{11}$$

The log likelihood is increased on each step and also the algorithm guaranteed to converge to a local maximum of the likelihood function.

The expectation and maximization steps are repeated until the difference between the estimated parameters of two consecutive steps are equal or inferior to a fixed threshold value ϵ .

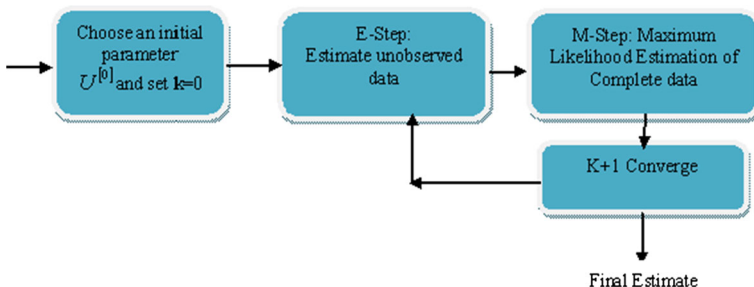


Fig. 2 Expectation maximization algorithm

2.3 Bone region extraction

The X-Ray image consists of three regions namely, Background, Skin and Bone. The EM algorithm segment the given X-ray image into three regions if $k = 3$, this technique is called region splitting. The EM algorithm is carried out in two steps: expectation step and maximization step using the Eqs. (7–11) to segment the given x-ray image. The result of EM algorithms contains three regions background, skin and bone from this only bone region is to detect the crack. Remove the background and skin region from the segmented image using the mask. Extract the bone region alone because the region of interest is only the bone region.

2.4 Crack identification using intensity variation technique

The hairline breakage on the bone region is considered here. Let P and Q be any two consecutive points in the X-ray image with coordinates (x_i, y_i) and (x_j, y_j) respectively. Let I_P and I_Q be the intensities of two pixels P and Q and let d_{PQ} be the Euclidean distance between them. The capacity function c_{PQ} is used to determine the variation among the neighboring pixels, which can be defined by the Eq. (12).

$$c_{PQ} = \frac{I_P I_Q}{d_{PQ}} \quad (12)$$

Here, the intensity at a crack site has a different intensity than the surrounding bone because a typical crack is marked by loss of bone. If the intensity variation is very much, that is larger than ε when compared with the surrounding pixels then the area is considered as crack. This is represented by the Eq. (13).

$$C_{PQ} \geq \varepsilon \quad (13)$$

where ε is the threshold limit.

3 Experimental procedure

The method has been tested on various grey level X-Ray images. All programs applied in simulating the algorithms are designed by MATLAB. A sample X-Ray image is shown in Fig. 3a. The given Bone X-ray image is filtered using the anisotropic diffusion technique with eight neighborhood pixel using the Eq. (1)–(6). The value of the integration constant Δs is assigned as 0.5. The diffusion constant, E_{diff} determines the value that triggers the smoothing process and it is assigned as 30. The diffusion function for wide regions over smaller ones is used here since a crack is a hairline breakage. The noise free image obtained by anisotropic diffusion is shown in Fig. 3b. Since the wavelets are used in description of edges as well as it retains minute pixels one level DWT is performed and LL component is used for further processing. The result after one level DWT is shown in Fig. 4. The X-Ray image consists of three regions namely: Background, skin and bone. Our area of interest is bone so EM algorithm is used to separate the regions and $k = 3$ is used to separate the given image into three regions such as bone, skin and Background region using the Eqs. (7)–(11). The segmented results are shown in Fig. 5. Using the masks of the EM algorithm from the input image the bone region is extracted, that output is shown in Fig. 6. The bone extracted image is then subjected to intensity variation calculation. The capacity value is calculated using Eq.



Fig. 3 a Original X-ray image (b) Noise free image obtained by anisotropic diffusion filter

(12), the intensity of each pixel is compared with its eight neighborhoods. If the pixels has a large intensity variation when compared to its neighbors that pixels are considered as hairline breakage displayed in Fig. 7. The inverse DWT is applied to get the actual position of the crack and it is shown in Fig. 8a. From the Fig. 8a the crack region is alone isolated and it is shown in

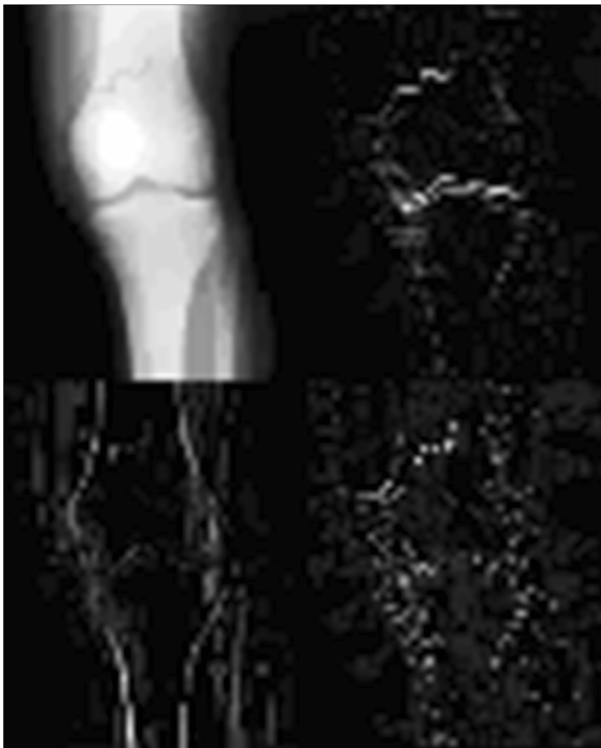


Fig. 4 One level decomposition using DWT



Fig. 5 Segmentation results of EM algorithm with $k = 3$

Fig. 8b. Finally the crack area is highlighted in Fig. 8c. The proposed work is tested for many sample X-Ray images. Some outputs for the sample X-Ray images are shown in Table 1.

3.1 Performance analysis

The proposed work is compared with “Automatic Crack Detection in Eggshell based on SUSAN Edge Detector Using Fuzzy Thresholding (FSUSAN)” [21] and “Crack detection in x-ray images using fuzzy index measure (FIM)” [9]. In order to perform the performance with the above said techniques the sensitivity and specificity [11, 25] calculation is performed using the Eqs. (14) and (15). Sensitivity or True Positive Rate is the ability of a test those with the Crack, whereas test Specificity or True Negative Rate is the ability of the test to correctly identify those without the crack.

$$\text{sensitivity} = \frac{TP}{(TP + FN)} \quad (14)$$

Fig. 6 Bone area extraction



Fig. 7 Crack identification using intensity variation calculation



$$\text{specificity} = \frac{TN}{(FP + TN)} \quad (15)$$

$$\text{Accuracy} = \frac{(TP + TN)}{(TP + TN + FP + FN)} \quad (16)$$



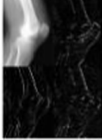
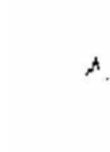



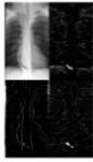




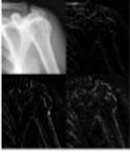
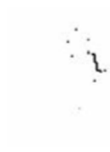



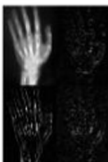


where

- TP* True Positive (correctly identified)
- FP* False Positive (incorrectly identified)
- TN* True Negative (correctly rejected)
- FN* False Negative (incorrectly rejected)



Fig. 8 **a** After invrse DWT, **(b)** crack region isolation and **(c)** crack highlighted in original image

Table 1 Sample experimental result

s.no	Original Image	Filtered image Using Anisotropic Diffusion	After DWT	Crack region Isolation	Crack region highlighted in the original image
1					
2					
3					
4					

The comparative results of sensitivity and specificity for the ten Patient’s sample image are given in Table 2. The Overall True Positive Rate (Sensitivity) is 0.8519 and the overall True Negative Rate (Specificity) is 0.9782. On seeing the results, the proposed method detects crack well than the previous work. The Accuracy of detection is also calculated using Eq. (16) and it is given in Table 2. Figure 9 shows the graphical chart of the Overall Accuracy rate of the three techniques. The overall accuracy rate of the proposed work is very high (98%) when compared with the other techniques. On seeing the sensitivity, specificity and accuracy the proposed work works than the other methods.

3.2 ROC analysis

Receiver Operating Characteristic (ROC) Curve Analysis [15] is important for medical diagnosis. In this the segmentation results of the proposed work are compared with other

Table 2 comparison of the proposed method with other two methods et al. [21] and Linda et al. [9]

Sl.no	Test image	Sensitivity		Specificity		Accuracy	
		Proposed Method	Mansoori et al. [21]	Proposed Method	Mansoori et al. [21]	Proposed Method	Mansoori et al. [21]
1	T1	0.8462	0.8279	0.8068	0.9898	0.9998	0.9877
2	T2	0.8387	0.7632	0.7856	0.9988	0.9984	0.9685
3	T3	0.7931	0.7290	0.7935	0.9878	0.9872	0.9364
4	T4	0.8233	0.8062	0.7992	0.9898	0.9910	0.9486
5	T5	0.8605	0.8168	0.8422	0.9988	0.9982	0.9693
6	T6	0.8596	0.7946	0.8093	0.9593	0.9587	0.9526
7	T7	0.8845	0.8376	0.8389	0.9483	0.9425	0.9187
8	T8	0.8678	0.7856	0.8047	0.9643	0.9617	0.8845
9	T9	0.8891	0.8393	0.8482	0.9785	0.9567	0.9123
10	T10	0.8567	0.8412	0.8382	0.9573	0.9876	0.8962

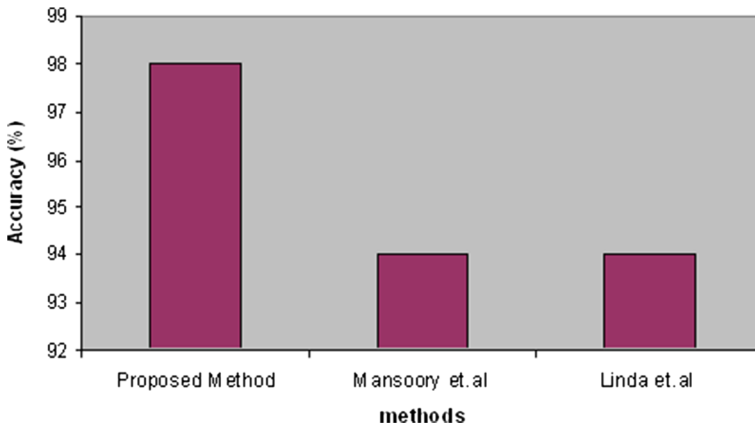


Fig. 9 Accuracy of detection

standard techniques by calculating the True Positives (TP), True Negatives (TN), False Positives (FP) and False Negatives (FN). The True Positive Rate (TPR) or the Sensitivity, and the False Positive Rate (FPR) or 1-specificity is calculated for the sample images. Figure 10 shows an ROC curve with Sensitivity vs 1-Specificity for all patients. The results also demonstrate that our new proposed technique has the ability to detect crack well when compared with the other techniques.

4 Conclusion

In this paper, a procedure for crack detection in Bone X-ray image based on the fusion of anisotropic diffusion and EM algorithm is proposed. The proposed algorithm produces

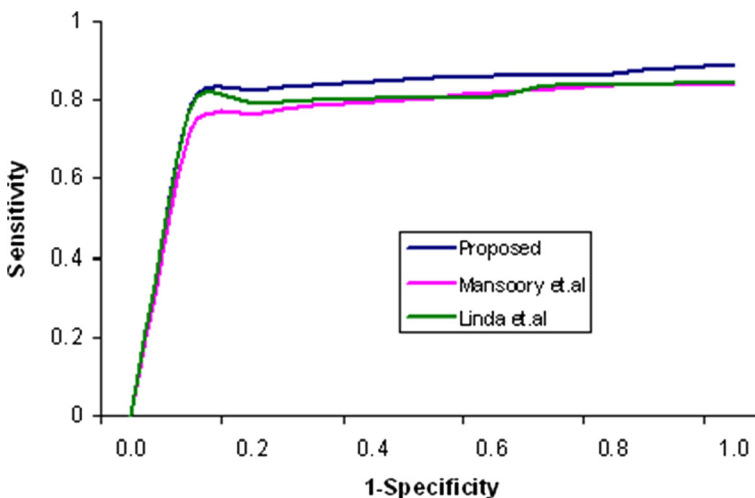


Fig. 10 ROC analysis

segmentations with high sensitivity and specificity. The overall sensitivity of the proposed method of all patients is 0.8519 and the overall true Negative Rate (Specificity) is 0.9782. The ROC analysis says that the proposed method provides better detections than two standard methods. We can improve the accuracy of crack detection by decreasing the error rates, this work can be extended on 3D images and the depth of the crack can also be calculated.

References

1. Bhandarkar SM, Datta GS, Yu JC, Chowdhury AS, Bhattacharya A, Figueroa R (2007) Hairline fracture detection using MRF and Gibbs sampling. *IEEE Int. Wkshp. on Applications of Computer Vision (WACV)*, pp 56–61
2. Bilmes JA (1998) A gentle tutorial of the EM algorithm and its application to parameter estimation for Gaussian mixture and hidden Markov models
3. Boykov Y, Jolly MP (2001) Interactive graph cuts for optimal boundary & region segmentation of objects in N-D images. In *Proceedings of International Conference on Computer Vision*, pp 105–112
4. Canny J (1986) A computational approach to edge detection. *IEEE Trans Pattern Anal Mach Intell* 8(6): 679–698
5. Chen Y, Howe T, Lum V, Leow W, Png M (2005) Combining classifiers for bone fracture detection in X-ray images. *IEEE Int. Conf. on Image Processing (ICIP)*, pp: 1149–1152
6. Datta G, Chowdhury AS, Bhandarkar SM, Yu JC (2006) Automated detection of stable fracture points in computed tomography image sequences. *IEEE Int. Symp. on Biomedical Imaging (ISBI)*, pp 1320–1323
7. Eksi Z, Dandil E, Cakiroglu M (2012) Computer aided bone fracture detection. *Signal Processing and Communications Applications Conference (SIU), 2012 20th. IEEE*, pp 1–4
8. Grau V, Mewes A, Alcaniz M, Kikinis R, Warfield SK (2004) Improved watershed transform for medical image segmentation using prior information. *IEEE Trans Med Imaging* 23(4):447–458
9. Harriet Linda C, Wiselin Jiji G (2011) Crack detection in X-ray images using fuzzy index measure. *Appl Soft Comput* 11(4):3571–3579
10. He JC, Leow WK, Howe TS (2007) Hierarchical classifiers for detection of fractures in X-ray images. *Int. Conf. on Computer Analysis of Images and Patterns (CAIP)*, vol. Springer LNCS 4673, pp: 962–969
11. Housami N, Irwig L, Simpson JM, McKessar M, Blome S, Noakes J (2003) Sydney breast imaging accuracy study: comparative sensitivity and specificity of mammography and sonography in young women with symptoms. *Am J Roentgenol* 180(4):935–940
12. Jacob NE, Wyawahare MV (2013) Survey of bone fracture detection techniques. *Int J Comput Appl* 71(17): 31–34
13. Jia Y, Jiang Y (2006) Active contour model with shape constraints for bone fracture detection. *Int. Conf. on Computer Graphics, Imaging and Visualization (CGIV)*, pp 90–95
14. Knowles G, Donnelley M, Hearn T (2008) A CAD system for long-bone segmentation and fracture detection. *IAPR Int. Conf. on Image and Signal Processing (ICISP)*, vol. Springer LNCS 5099, A. Elmoataz et al. (Eds.), pp 153–162
15. Krupinski EA (2017) Receiver operating characteristic (ROC) analysis. *Frontline Learning Research* 5(3): 31–42 ISSN 2295-3159
16. Kwon G-R, Basukala D, Lee S-W, Lee KH, Kang M (2016) Brain image segmentation using a combination of expectation-maximization algorithm and watershed transform. *International Journal of Imaging Science and Technology* 26(3):225–232
17. Leow WK, Howe TS, Yap DWH, Chen Y, Png MA (2004) Detecting femur fractures by texture analysis of trabeculae. *IEEE Int. Conf. on Pattern Recognition (ICPR)*, pp 730–733
18. Lim SE, Xing Y, Chen Y, Leow WK, Howe TS, Png MA (2004) Detection of femur and radius fractures in X-ray images. In *Proceedings 2nd International Conference on Advances in Medical Signal and Information Processing*
19. Mahendran SK, Santhosh Baboo S (2011) An enhanced tibia fracture detection tool using image processing and classification fusion techniques in X-ray images. *Global J Comp Sci Technol* 11(14 Version 1.0):22–28
20. Mahmoodi S (2011) Anisotropic diffusion for noise removal of band pass signals. *Elsevier Signal Processing* 91:1298–1307

21. Mansoori MS, Ashtiyani M, Sarabadani H (2012) Automatic crack detection in eggshell based on SUSAN edge detector using fuzzy thresholding. *World Applied Sciences Journal* 18(11):1602–1608
22. McInerney T, Terzopoulos D (1996) Deformable models in medical image analysis: a survey. *Published Medical Image Analysis* 1(2):91–108
23. Mendrik A, Vonken E, Rutten A, Viergever M, van Ginneken B (2009) Noise reduction in computed tomography scans using 3D anisotropic hybrid diffusion with continuous switch. *IEEE Trans Med Imaging* 28(10):1585–1594
24. Panchasara C, Joglekar A (2015) Application of image segmentation techniques on medical reports. *International Journal of Computer Science and Information Technologies* 6(3):2931–2933
25. Reitsmaa JB, Glasa AS, Rutjesa AWS, Scholtenb RJPM, Bossuyta PM, Zwindermana AH (2005) Bivariate analysis of sensitivity and specificity produces informative summary measures in diagnostic reviews. *J Clin Epidemiol* 58(10):982–990
26. Rogowska J (2000) Overview and fundamentals of medical image segmentation. In: Bankman IN (ed) *Handbook of medical imaging, processing and analysis*, vol 5. Academic Press, Cambridge, pp 69–85
27. Sezgin M, Sankur B (2004) Survey over image thresholding techniques and quantitative performance evaluation. *J Electron Imaging* 13(1):146–165
28. Sharan V, Keshari N, Mondal T (2014) Biomedical image denoising and compression in wavelet using MATLAB. *International journal of Innovative Science and Modern Engineering (IJISME)*, ISSN:2319-6386 2(6):9–13
29. Thakare P (2011) A study of image segmentation and edge detection techniques. ISSN: 0975–3397, 3(2): 899–904
30. Tian TP, Chen Y, Leow WK, Hsu W, Howe TS, Png MA (2003) Computing. Neckshaft angle of femur for X-ray fracture detection. In: Petkov N, Westenberg MA (eds) *CAIP 2003*. LNCS, 2756. Springer, Heidelberg, pp 82–89
31. Yogeswara Rao K, James Stephen M, Siva Phanindra D (2012) Classification based image segmentation approach. *IJCST*. ISSN: 2229–4333, 3(1):658–659



C. Harriet Linda received her B.E. and M.E. degrees in Computer Science and Engineering in 1999 and 2007 respectively. She is currently pursuing her PhD Degree. She has published some research papers in international conferences and journals. Her research interests include Computer Vision, image processing and image analysis based on image segmentation and pattern recognition.



Dr. G. Wiselin Jiji received her B.E. and M.E. degrees in Computer Science and Engineering in 1994 and 1998 respectively. In 2008, she received the Doctoral degree in Information & Communication Engineering from the Anna University Chennai. She received four national awards and two state awards. She published a lot of papers in leading journals. Under her guideline four R&D projects are going on. Her research interests include image processing and image analysis based on image segmentation and pattern recognition.